Nonlinear Climate and Hydrological Responses to Aerosol Effects

YI MING AND V. RAMASWAMY

Geophysical Fluid Dynamics Laboratory, Princeton, New Jersey

(Manuscript received 4 December 2007, in final form 30 July 2008)

ABSTRACT

The equilibrium temperature and hydrological responses to the total aerosol effects (i.e., direct, semidirect, and indirect effects) are studied using a modified version of the Geophysical Fluid Dynamics Laboratory atmosphere general circulation model (AM2.1) coupled to a mixed layer ocean model. The treatment of aerosol–liquid cloud interactions and associated indirect effects is based upon a prognostic scheme of cloud droplet number concentration, with an explicit representation of cloud condensation nuclei activation involving sulfate, organic carbon, and sea salt aerosols. Increasing aerosols from preindustrial (1860) to present-day (1990) levels leads to a decrease of 1.9 K in the global annual mean surface temperature. The cooling is relatively strong over the Northern Hemisphere midlatitude land owing to the high aerosol burden there, while being amplified at high latitudes. When being subject to aerosols and radiatively active gases (i.e., well-mixed greenhouse gases and ozone) simultaneously, the model climate behaves nonlinearly; the simulated increase in surface temperature (0.55 K) is considerably less than the arithmetic sum of separate aerosol and gas effects (0.86 K). The thermal responses are accompanied by the nonlinear changes in cloud fields, which are amplified owing to the surface albedo feedback at high latitudes. The two effects completely offset each other in the Northern Hemisphere, while gas effect is dominant in the Southern Hemisphere. Both factors are crucial in shaping the regional responses. Interhemispheric asymmetry in aerosol-induced cooling yields a southward shift of the intertropical convergence zone, thus giving rise to a significant reduction in precipitation north of the equator, and an increase to the south. The simulations show that the change of precipitation in response to the simultaneous increases in aerosols and gases not only largely follows the same pattern as that for aerosols alone, but that it is also substantially strengthened in terms of magnitude south of 10°N. This is quite different from the damping expected from adding up individual responses, and further indicates the nonlinearity in the model's hydrological response.

1. Introduction

Anthropogenic aerosols from burning fossil fuels and biomass affect the earth's radiation balance in multiple ways. They scatter and absorb shortwave (SW) and longwave (LW) radiation in the clear sky (the direct effect; e.g., Haywood and Ramaswamy 1998). Atmospheric warming exerted by absorbing aerosols (e.g., black carbon) facilitates dissipation of clouds through evaporating droplets (the semidirect effect; e.g., Hansen et al. 1997). Water-soluble aerosol particles (e.g., sulfate and sea salt) participate in cloud formation by acting as cloud condensation nuclei (CCN), and thus are important for determining microphysical and radiative properties of clouds. Smaller droplets resulting from enhanced CCN concentrations are the cause of higher cloud albedo (the first indirect effect; Twomey 1977) and longer cloud lifetime (the second indirect effect; Albrecht 1989). Note that the term ''indirect effects'' as used in this study refers to those resulting from the interactions between aerosols and liquid clouds only (i.e., no ice cloud effects).

It is clear from the above descriptions that the thermodynamic states of the atmosphere and cloud fields need to be able to adjust for the semidirect and total indirect effects to manifest. These effects do not conform to the rigorous definition of radiative forcing (Ramaswamy et al. 2001). One may argue that they are among the aerosol-induced feedback mechanisms involving clouds. This is a fundamental difference from the aerosol direct effect, which acts as forcing. Numerous studies have calculated top-of-the-atmosphere (TOA) flux changes resulting from indirect effects comparable to the forcing by the well-mixed greenhouse gases

Corresponding author address: Yi Ming, 201 Forrestal Rd., Princeton University, NOAA/Geophysical Fluid Dynamics Laboratory, Princeton, NJ 08542.
E-mail: Yi.Ming@noaa.gov

DOI: 10.1175/2008JCLI2362.1

(WMGGs) in magnitude (but opposite in sign) using atmospheric general circulation models (AGCMs) with fixed sea surface temperatures (SSTs; e.g., Lohmann and Feichter 2005; Ming et al. 2006). Despite a few early efforts (e.g., Hansen et al. 2005; Takemura et al. 2006), more research is needed to investigate the nature of the transient climate response with a fully coupled atmosphere–ocean GCM (AOGCM), which implements ocean dynamics. A specific issue is to what extent aerosol effects are able to offset or even reverse WMGG-induced warming. This is crucial for constraining climate sensitivity from the observed temperature trend (Andreae et al. 2005) and for studying global and regional climate change.

As an integral part of the earth's climate system, the hydrological cycle is also subject to aerosol impacts. Aerosols are effective in reducing SW radiation reaching the surface, and thus in slowing down evaporation and precipitation (Ramanathan et al. 2001). Any change in the thermodynamic state of the atmosphere can result in variations in precipitation pattern. For example, the uneven heating (or cooling) of two hemispheres can shift the position of the intertropical convergence zone (ITCZ) with a direct bearing on monsoons (Chen and Ramaswamy 1996; Ramaswamy and Chen 1997; Rotstayn and Lohmann 2002; Broccoli et al. 2006). The possible influence of aerosols on the strength and pattern of the hydrological cycle can be properly studied only with AOGCMs.

As a less expensive alternative to using a fully coupled AOGCM, which requires multicentury control runs, a number of studies have utilized AGCMs coupled to mixed layer ocean models for assessing the equilibrium climate response to aerosols (Williams et al. 2001; Rotstayn and Penner 2001; Rotstayn and Lohmann 2002; Feichter et al. 2004; Krisjánsson et al. 2005; Jones et al. 2007). The main weakness of mixed layer models is the lack of ocean dynamics, which has been shown to be important for understanding the climate response to aerosols simulated in fully coupled models (Delworth and Dixon 2006; Rotstayn et al. 2007; Cai et al. 2007). Typically, cloud droplet number concentration (N_d) was diagnosed from aerosol concentration either based on the empirical relationship (e.g., Boucher and Lohmann 1995) or based on the Köhler equation at a fixed supersaturation. In contrast, the study by Feichter et al. (2004) has taken the field forward by treating N_d as a prognostic variable, whose evolution is subject to a variety of sources and sinks, in conjunction with online simulation of aerosol concentration, thus representing a more realistic approach to modeling indirect effects.

This study examines the thermal, radiative, and hydrological responses to aerosol effects, and the nonlinearity arising in adding the responses to changes in aerosols and radiatively active gases (i.e., WMGG and ozone), using a modified version of the Geophysical Fluid Dynamics Laboratory (GFDL) AGCM (AM2.1), with a fully self-consistent prognostic cloud scheme (Ming et al. 2007). The roles of feedback mechanisms and thermodynamic processes in shaping the responses are discussed.

2. Model description and design of experiments

The coupled atmosphere–mixed layer ocean model used in this study has separate atmosphere, mixed layer ocean, sea ice, and land components, which exchange fluxes through a coupler module. It is nearly identical to the slab model SM2.1 used in Stouffer et al. (2006) for evaluating the equilibrium climate sensitivity to doubling CO_2, other than the modifications made to the atmospheric component for incorporating aerosol indirect effects. A series of papers have been published to document the formulation and performance of the components in the GFDL AOGCM, namely, Climate Model versions 2.0 and 2.1 (CM2.0 and CM2.1, respectively; see Delworth et al. 2006; Stouffer et al. 2006). Here, only the aspects of the model most relevant for understanding the methodology and results of this study are described. Readers should refer to the above references for additional detail.

The atmospheric component is built upon a finite-volume (FV) dynamical core (Lin 2004), and the model physics is parameterized mostly following the GFDL Global Atmospheric Model Development Team (2004). Ming et al. (2007) developed a prognostic scheme of N_d that uses model-resolved updraft velocity for driving CCN activation, and explicitly considers a set of dynamical and microphysical sources and sinks in convective and large-scale stratiform clouds. The parameterization of CCN activation (Ming et al. 2006) takes into account the size distributions and chemical compositions of multiple aerosol types, namely, sulfate, organic carbon, and sea salt. The prognostic N_d is used to compute cloud optical depth and large-scale precipitation rate. An implementation of the scheme in an earlier version of AGCM (based on a B grid dynamical core) with prescribed SST yielded a global annual mean flux change of $-1.8\ \mathrm{W}^{-2}$ resulting from aerosol indirect effects (Ming et al. 2007). Here, the same scheme is implemented in the FV-based atmospheric component. It is found that the differences in the dynamical core and model parameters cause little change in the calculated flux change. The climatology of tropospheric aerosols and ozone is prescribed offline based on monthly mean results from the Model for Ozone and Related Chemical Tracers

TABLE 1. PI and PD atmospheric concentrations of WMGG and global annual mean burdens of ozone and aerosols.

Species	PI	PD
CO_2 (ppm)	286	353
CH_4 (ppb)	806	1694
N_2O (ppb)	275	309
CFC11 (ppt)	0	263
CFC12 (ppt)	0	477
CFC113 (ppt)	0	77
HCFC22 (ppt)	0	91
Tropospheric ozone (Tg)	253.6	366.9
Sulfate (Tg S)	0.22	0.81
Organic carbon (Tg C)	0.17	1.36
Black carbon (Tg C)	0.02	0.28

(MOZART) chemical transport model (Horowitz 2006). The distributions of stratospheric ozone are prescribed according to Randel and Wu (1999). One shortcoming of using prescribed aerosols is the inability to capture the impacts of changing dynamics and meteorology on aerosol burdens.

The ocean component has a uniform mixed layer depth of 50 m (Manabe and Stouffer 1980). The temperature is driven by the net heat flux at the surface as calculated in the atmospheric component. Ocean heat transport is not explicitly considered because of the lack of ocean dynamics. Its role is mimicked using heat flux adjustment derived from a simulation forced by observed SST and sea ice (Hansen et al. 1984). The sea ice component is a dynamical model with three vertical layers (one representing snow and two representing ice; Winton 2000). It implements a scheme for prognosticating five different ice thickness categories and open water. The land component is the land dynamics model (Milly and Shmakin 2002). When snow cover is present, its depth determines the land surface albedo.

Because the equilibrium climate responses to the increases in forcing agents (i.e., aerosols and/or radiatively active gases) from 1860 [preindustrial (PI)] to 1990 [present day (PD)] are the subject of this study, a PI control case is desirable so that perturbations can be made in the proper order. Because no observed SST and sea ice climatology exists for PI, flux adjustment is computed from a 20-yr simulation forced by observed PD SST and sea ice with radiatively active gases and aerosols set at PI levels (Table 1). It is applied to create the PI control run (CONT), which is then perturbed by changing to either PD (1990) aerosols (AERO) or PD radiatively active gases (GAS), or both (BOTH). Note that the simulated climatology in BOTH is in reasonably good agreement with the PD observations, with the differences in SST mostly within 0.5 K as a consequence of the relatively small net forcing (see discussion below). The control and perturbation cases are run for 80 model years each, and the last 20 yr are analyzed. The time series of global annual mean surface temperature in four cases are plotted in Fig. 1. Forcing calculations show a global annual mean instantaneous tropopause forcing of 2.5 W m^{-2} for radiatively active gases and an instantaneous TOA forcing of -0.43 W m^{-2} for aerosol direct effect. The TOA flux change resulting from aerosol indirect effects amounts to -1.7 W m^{-2}, which is well within the wide range of published estimates of indirect effects (from -1.1 to -2.3 W m^{-2}; Lohmann and Feichter 2005). Even so, it does reduce the net forcing in the industrial era to a level that may be hard to reconcile with the observed twentieth-century temperature trend. A simulation of transient climate response with AOGCM may shed more light on this issue.

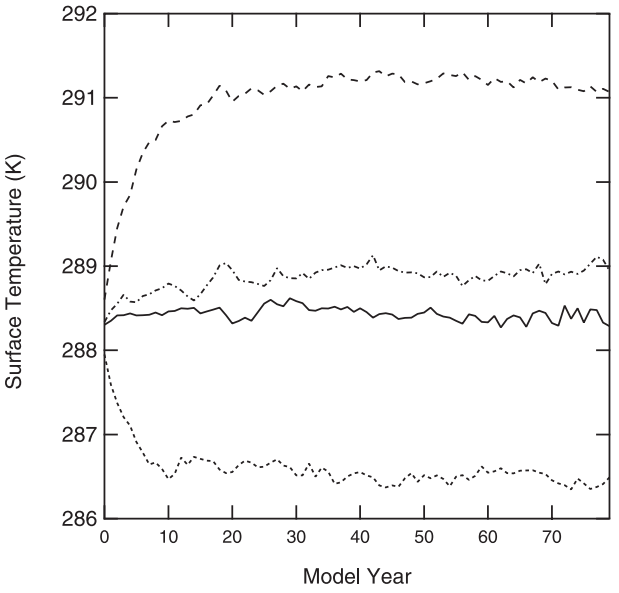

FIG. 1. Time series of global annual mean surface temperature (K) in CONT (solid line), AERO (dotted line), GAS (dashed line), and BOTH (dashed–dotted line).

3. Results

a. Response to aerosol effects

As shown in Fig. 1, the model climate (as represented by surface temperature) shifts gradually from the CONT to different equilibrium states in response to increased aerosols and/or radiatively active gases. The differences in equilibrium surface temperature between perturbation cases and CONT (the former minus the latter) are listed in Table 2. Relative to CONT, anthropogenic aerosols (AERO) cause the surface to cool by 1.9 K globally. Two separate experiments (not shown here) suggest

TABLE 2. Differences in surface temperature (K) between perturbation cases and CONT.

	Global	NH land	NH ocean	SH land	SH ocean
AERO	−1.90	−2.93	−2.02	−2.06	−1.27
GAS	2.76	3.74	2.60	3.33	2.27
BOTH	0.55	0.03	0.00	1.19	1.07

that direct and semidirect effects give rise to a surface cooling of 0.62 K, while indirect effects cause a cooling of 1.3 K. Thus, the cooling caused by the combined aerosol effects mainly is due to indirect effects. Anthropogenic radiatively active gases warm the surface by 2.8 K. When combined, aerosols and radiatively active gases drive the climate to a state warmer than CONT in terms of global annual mean surface temperature, suggesting that warming from radiatively active gases outweighs cooling from aerosols as expected from the respective magnitudes when acting separately. However, the net warming of 0.55 K in BOTH is considerably less than the arithmetic sum of the changes in AERO and GAS (0.86 K), indicating some degree of nonlinearity characteristic of the model's thermal response. The two hemispheres behave differently in this aspect. The responses to aerosols and radiatively active gases are mostly linearly additive in the Southern Hemisphere (SH), while the Northern Hemisphere (NH) claims virtually all the nonlinearity (Table 2). This issue will be discussed in detail in section 3b.

Despite the highly regional nature of the aerosol burden, the resulting surface cooling in AERO spreads across the whole globe with local maxima (Fig. 2). The strongest cooling is located over, but not limited to, the NH midlatitude industrial regions (namely, East Asia, Europe, and the northeastern United States) and the biomass-burning region in South America, all of which are under the influence of heavy aerosol burden. Remote regions, such as the Southern Ocean, experience moderate cooling despite scarce anthropogenic aerosols. This highlights how effective the atmosphere is in spreading local perturbations via heat transport. (The role of ocean heat transport is not explicitly considered in this study because of the lack of ocean dynamics in the mixed layer model.) Nonetheless, NH still cools to a greater extent than SH partly owing to the higher aerosol burden. (The influence of interhemispheric asymmetry in the thermal response on the position of the ITCZ and precipitation will be discussed later.) As a general trend, the cooling is significantly amplified at high latitudes. For example, some of the strongest cooling takes place in Siberia and the east part of Canada. As explained later, surface albedo feedback contributes to this characteristic.

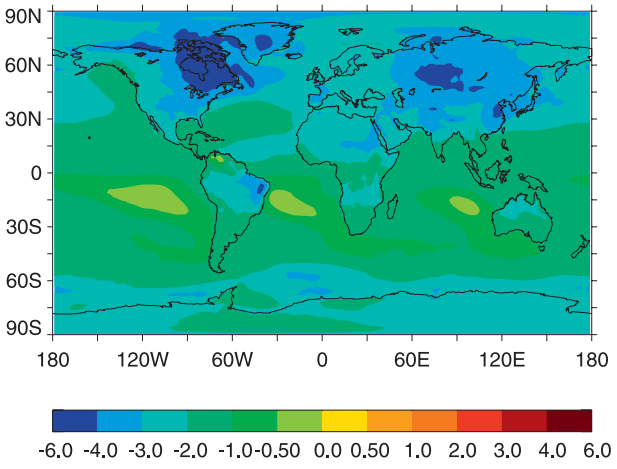

FIG. 2. Geographical distribution of annual mean difference in surface temperature (K; AERO minus CONT).

The vertical distribution of annual zonal mean difference in air temperature is depicted in Fig. 3. Increased aerosols lead to a colder troposphere, but a largely warmer stratosphere in AERO. This is generally consistent with the pattern of the response to indirect effects in Williams et al. (2001), and is opposite to the response to radiatively active gases characteristic of warming in the troposphere and cooling in the stratosphere (e.g., Stouffer et al. 2006). The tropospheric response also varies with altitude and latitude. The cooling in NH is stronger than that in SH because of the higher aerosol burden. At the low latitudes, the strongest cooling takes place between 200 and 400 mbar, instead of at the surface (as is true for the mid- and high latitudes), resulting from reduced convective heating. As a consequence, moist adiabatic lapse rate is preserved.

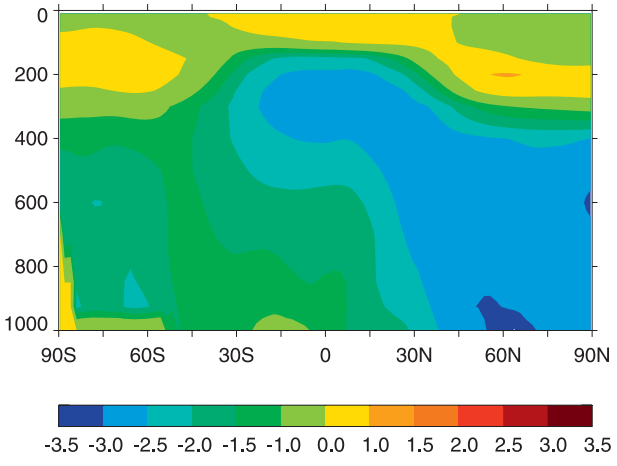

FIG. 3. Vertical distribution of annual zonal mean difference in air temperature (K; AERO minus CONT).

TABLE 3. Global annual mean differences between perturbation cases and CONT.

	AERO	GAS	BOTH
Surface temperature (K)	−1.9	2.8	0.55
SW TOA all-sky flux (W m^{-2})	−3.4	2.1	−1.3
SW TOA clear-sky flux (W m^{-2})	−3.6	2.0	−1.7
SW TOA cloudy-sky flux (W m^{-2})	0.19	0.10	0.47
LW TOA all-sky flux (W m^{-2})	3.4	−2.2	1.3
LW TOA clear-sky flux (W m^{-2})	4.0	−2.5	1.8
LW TOA cloudy-sky flux (W m^{-2})	−0.60	0.37	−0.47
SW surface all-sky flux (W m^{-2})	−4.4	−0.02	−4.1
LW surface all-sky flux (W m^{-2})	−0.63	3.0	1.9
LWP (g m^{-2})	5.3	1.0	7.0
Total cloud amount (%)	1.0	−1.4	−0.05
Evaporation (mm day^{-1})*	−0.17	0.14	−0.04

* The values are also applicable to precipitation owing to global-scale balance between evaporation and precipitation.

The model's equilibrium response in all-sky SW and LW radiation flux at TOA ought to balance out each other on the global scale. Although this is true for all of the perturbation cases (Table 3), they adjust to new equilibrium states in different ways. A higher aerosol burden in AERO leads to an increase of 3.4 W m^{-2} in outgoing SW TOA all-sky flux, which registers as a deficit in the total radiation balance (Table 3). In contrast, outgoing SW TOA all-sky flux reduces by 2.1 W m^{-2} in response to higher concentrations of radiatively active gases in GAS. This results mainly from the changes in surface albedo and clouds. When the model is subject to increased aerosols and radiatively active gases simultaneously (BOTH), the same field increases by 1.3 W m^{-2}. The clear-sky radiation flux is computed by calling the model's radiation code in the absence of clouds for diagnostic purpose. The difference between all- and clear-sky fluxes is defined as the cloudy-sky flux. A breakdown of the all-sky flux change into clear- and cloudy-sky components suggests the dominance of the former in the global mean sense. However, this by no means rules out significant roles of clouds in affecting regional radiation balance as explained later.

The geographical distributions of the differences (AERO minus CONT) in SW TOA clear-sky and cloudy-sky fluxes are plotted in Fig. 4. The radiative cooling in clear-sky SW (i.e., more outgoing radiation) spans almost all latitudes, but not without large spatial variations in strength. The strongest radiative cooling (greater than 5 W m^{-2}) is found mainly north of 30°N and south of 60°S, encompassing the high-latitude regions with snow/ice cover as well as the NH midlatitude land and oceans affected by heavy anthropogenic aerosol burden. Relatively mild radiative cooling (1–3 W m^{-2}) occurs over South America and central Africa and the oceanic regions downwind. As shown in Fig. 5, higher surface albedo resulting from an increased amount of sea ice and snowfall is accompanied by the SW cooling over the high-latitude land and oceans and over the NH midlatitude land.

SW TOA cloudy-sky flux responds to increased aerosols in two distinct modes: it increases north of 45°N and south of 45°S, but decreases between 45°N and 45°S. This behavior is generally consistent with the change in liquid water path (LWP; Fig. 6). For example, among the three NH industrial regions with high aerosol burden, LWP increases substantially over East Asia and the northeastern United States (which are mostly south of 45°N). This is due to both aerosol indirect effects and dynamic and thermodynamic changes in clouds. In contrast, the increase in LWP over Europe, a large part of which lies north of 45°N, is much less significant than suggested by the simulations with prescribed SST and snow/ice cover (see Fig. 17 in Ming et al. 2007). Lower LWP north of 45°N has an effect of reducing reflected SW TOA all-sky flux, thus partially compensating for the radiative imbalance arising from surface albedo feedback.

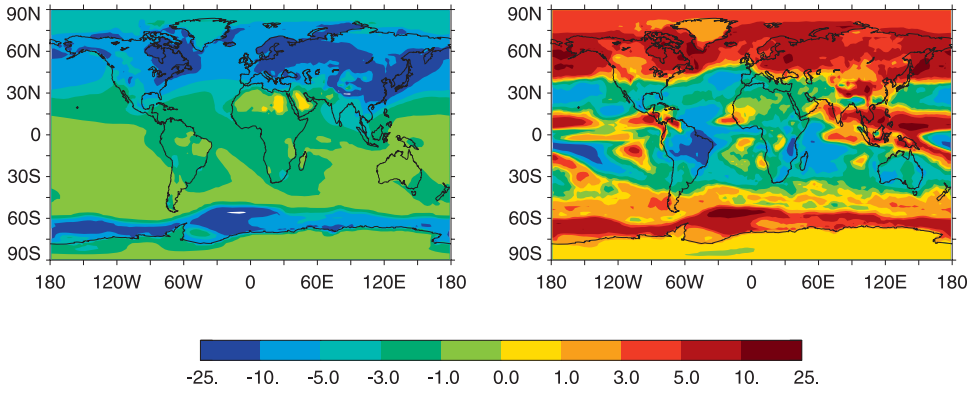

FIG. 4. Geographical distribution of annual mean difference between SW TOA (left) clear-sky and (right) cloudy-sky fluxes (W m^{-2}; AERO minus CONT).

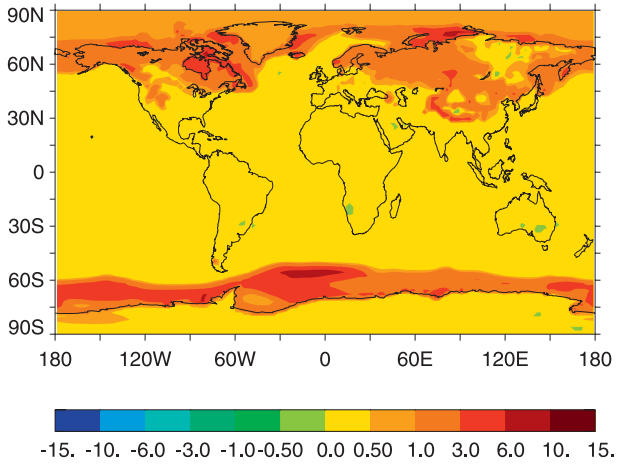

FIG. 5. Geographical distribution of annual mean difference in surface albedo (%; AERO minus CONT).

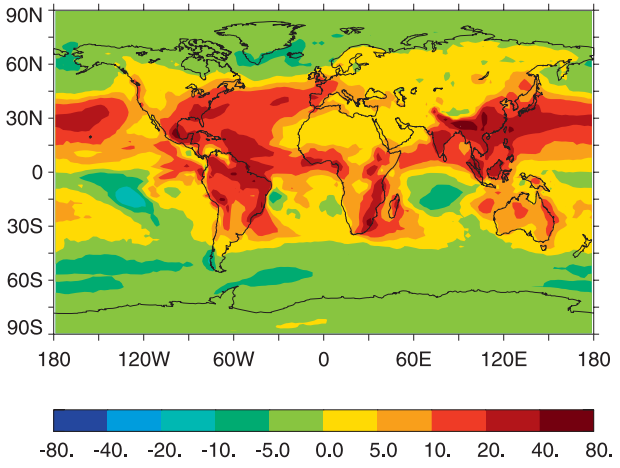

FIG. 6. Geographical distribution of annual mean difference in LWP (g m^{-2}; AERO minus CONT).

Two thermodynamic effects are crucial for understanding the decrease in LWP at these relatively high latitudes. As formulated in the large-scale cloud scheme (Tiedtke 1993) used in the model, the production rate of total cloud condensate is proportional to dq_s/dT (q_s is the mass mixing ratio of saturated water vapor), which increases monotonically with temperature (T). In the temperature range typical of high latitudes (from 0° to −30°C), the relative increase in dq_s/dT is averaged at 8% K^{-1}. Because large-scale ascent that drives cloud formation is little changed, the large-scale source of cloud condensate would reduce approximately by 24% owing to a NH high-latitude cooling of around 3 K in AERO. The second effect arises from the fact that colder temperatures favor the partitioning of cloud condensate into ice at the expense of liquid in mixed-phase clouds. Because the relative decrease in LWP is around 30% in AERO, the dq_s/dT effect should be more important than the freezing effect in changing LWP at high latitudes where large-scale stratiform clouds are dominant. This also explains the simultaneous decrease in ice water path (IWP; Fig. 7), since the freezing effect alone would lead to an increase in IWP if total condensate is unchanged.

As discussed in the following section, the interhemispheric asymmetry in thermal response (i.e., NH cools more than SH) causes a southward shift of ITCZ. As a result, cloud amount reduces north of the equator, while increasing south (not shown). The pattern of the response in SW TOA cloudy-sky flux in the tropics generally follows that in cloud amount; increased cloud cover enhances reflection, and thus reflected SW TOA flux.

An analysis of surface energy budget reveals that anthropogenic aerosols reduce global annual mean SW surface all-sky flux by 4.4 W m^{-2}, while the impact of radiatively active gases is virtually entirely in LW with a net increase of 3.0 W m^{-2} (Table 3). The geographical distribution of the difference in SW surface all-sky flux shows that the strongest reduction typically ranging from 5 to 20 W m^{-2} occurs over the NH midlatitude industrial and SH biomass-burning regions and the neighboring oceans (Fig. 8). The less SW radiation energy that is available at the surface directly translates into reduced evaporation, particularly over the oceanic regions downwind of aerosol source regions (not shown). This amounts to a reduction of 0.17 mm day^{-1} on the global scale. In comparison, anthropogenic radiatively active gases accelerate evaporation by trapping more LW surface energy. This occurs almost all over the oceans (not shown), and leads to a global annual increase of 0.14 mm day^{-1}. The opposing effects of aerosols and radiatively active gases largely cancel out in

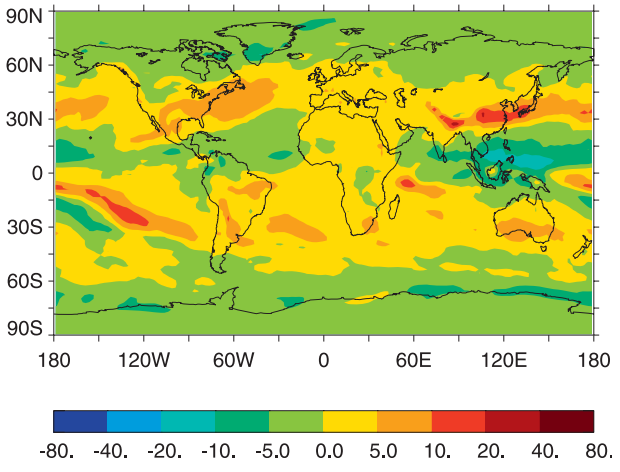

FIG. 7. Geographical distribution of annual mean difference in IWP (g m^{-2}; AERO minus CONT).

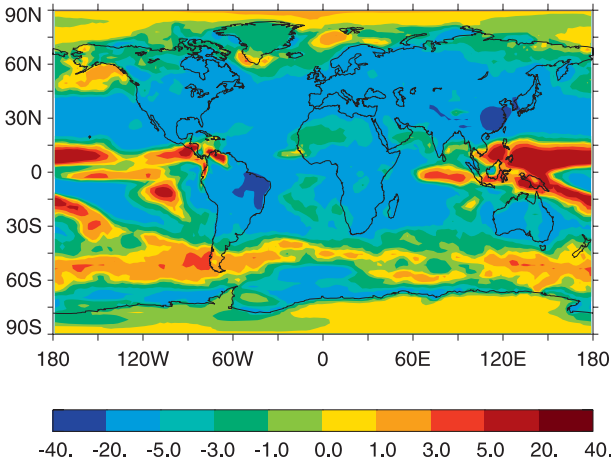

FIG. 8. Geographical distribution of annual mean difference in SW surface all-sky flux (W m^{-2}; AERO minus CONT).

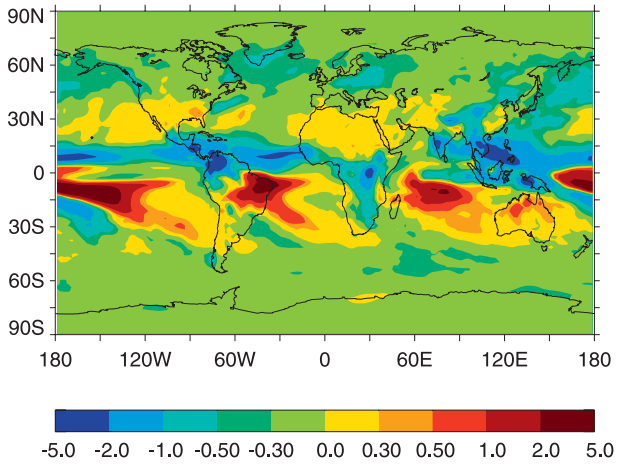

FIG. 9. Geographical distribution of annual mean difference in precipitation (mm day^{-1}; AERO minus CONT).

SH for BOTH, while the net effect is less evaporation in the tropics and NH with a global annual mean of -0.04 mm day^{-1}.

As a result of the balance between evaporation and precipitation on the global scale, these global annual mean values are also applicable to precipitation. However, their geographical distributions differ substantially (Fig. 9). Because NH cools more than SH resulting from a higher aerosol burden (Fig. 3), ITCZ undergoes a southward shift, which gives rise to substantially less precipitation north of the equator and more to the south. Particularly, Southeast and South Asia, sub-Saharan Africa, and Central America are among the regions most affected by this altered precipitation pattern. This change in precipitation pattern was found in other studies (Williams et al. 2001; Rotstayn and Lohmann 2002; Feichter et al. 2004; Krisjánsson et al. 2005), and was invoked as a possible cause of Sahelian drought in Rotstayn and Lohmann (2002). The jet streams show a pronounced southward shift over the Pacific as a consequence of stronger cooling of NH (Mitchell and Johns 1997; Raisanen 1998). This causes the NH midlatitude storm track to move southward as well, resulting in a modest decrease in precipitation north of 45°N and an increase south. Krisjánsson et al. (2005) related the same phenomenon to the changes in sea level pressure over the Arctic.

b. *Nonlinearity in total response to aerosols and gases*

To study to what extent the impacts of aerosols and radiatively active gases are linearly additive, BOTH is compared with the arithmetic sum of AERO and GAS (AERO + GAS) in terms of zonal mean values for different fields in Figs. 10–13 . If the fields in BOTH are assumed to be independent of those in CONT, one standard deviation of the difference between BOTH and CONT for a particular field X $[\sigma(X_{\mathrm{BOTH}} - X_{\mathrm{CONT}})]$ can be calculated as $\sqrt{\sigma(X_{\mathrm{BOTH}})^2 + \sigma(X_{\mathrm{CONT}})^2}$. The 95% confidence intervals with t tests are denoted as error bars for BOTH and the arithmetic sum in the figures as a measure of unforced model variability. The results consistently show statistically significant nonlinearity in NH, where aerosol effects are concentrated. For example, the zonal mean surface temperature in BOTH is always lower than expected from adding up AERO and GAS, and their respective confidence intervals do not overlap (Figs. 10). Relatively modest nonlinearity exists at the

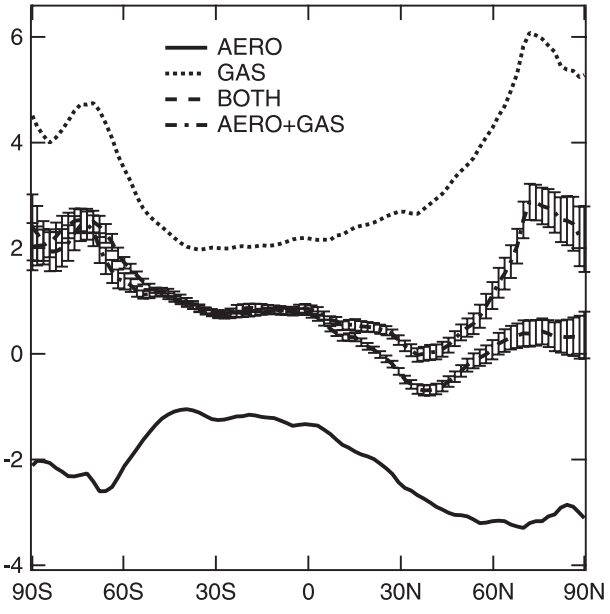

FIG. 10. Zonal mean differences in surface temperature (K; perturbation cases minus CONT).

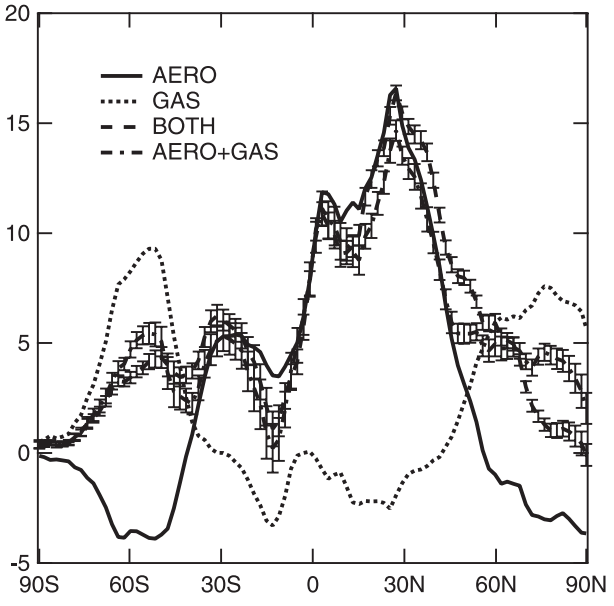

FIG. 11. Zonal mean differences in LWP (g m^{-2}; perturbation cases minus CONT).

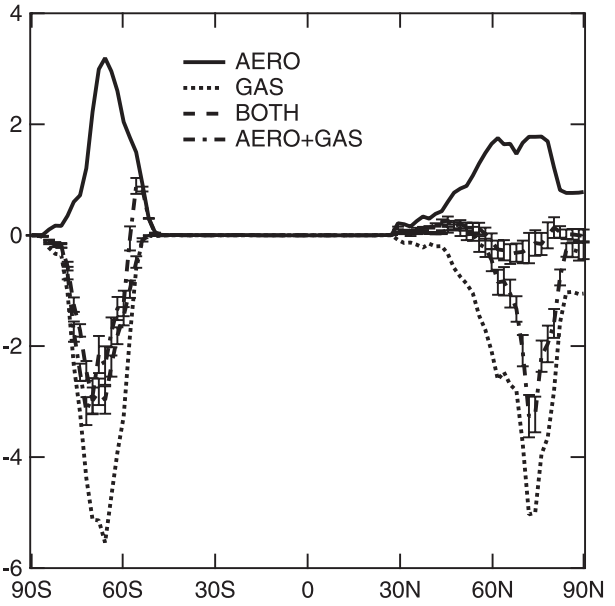

FIG. 12. Zonal mean differences in surface albedo (%; perturbation cases minus CONT).

NH low and midlatitudes, where surface albedo effect is small, and is mainly associated with the response in cloud fields. As shown in Fig. 11, the increases in LWP in BOTH is greater than the arithmetic sum of AERO and GAS at these latitudes, thus giving rise to stronger cooling. This may be due to changes in circulation, which in return affects the distribution of clouds in a nonlinear fashion. Currently, dynamically induced cloud response is poorly understood (e.g., Soden and Held 2006; Wyant et al. 2006). Aerosols, which modulate cloud fields by altering microphysics, can also contribute to the nonlinear cloud response because the nonlinearity in LWP arises only at these latitudes where anthropogenic aerosols are present.

The overestimates by assuming linearity are particularly large (approximately 2 K) at the NH high latitudes. Surface albedo feedback is at least partly responsible for the amplification of high-latitude thermal response in both hemispheres. Figure 12 shows that although the increase in surface albedo in AERO is not enough to compensate for the decrease in GAS, the simulated zonal mean change in BOTH is almost negligible compared to the large reduction indicated by the arithmetic sum. Does this mean that the nonlinear thermal response results from surface albedo feedback? The simulations show that the individual responses in AERO and GAS are linearly additive at the SH high latitudes. This suggests that surface albedo feedback alone will give rise to linear thermal response. The differences between the arithmetic sum and BOTH in Fig. 10 (which are thought of as a measure of nonlinearity) at the NH high latitudes are approximately 3 times that at the midlatitudes. The magnitude is comparable to the amplification in AERO and GAS. Moreover, the calculations based on the partial radiative perturbation (PRP) method (Wetherald and Manabe 1988) indicate that the strength of albedo feedback (defined as the change in

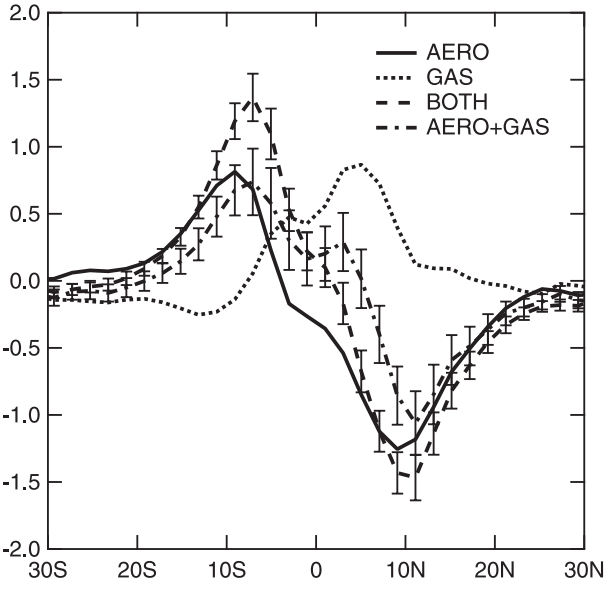

FIG. 13. Zonal mean differences in precipitation (mm day^{-1}; perturbation cases minus CONT).

TOA radiative flux solely resulting from the change in surface albedo normalized by the change in T_s) is almost identical for AERO and GAS. These further support the fact that surface albedo feedback behaves linearly. Therefore, surface albedo feedback is not the root cause of the nonlinear thermal response at NH high latitudes, but instead it is a mechanism that amplifies the response. Alexeev et al. (2005) and Winton (2006) showed that other processes can also contribute to the high-latitude amplification. However, it is difficult without comparisons with other models or more idealized experiments to have a high level of confidence in the robustness of the manner in which the nonlinearity is manifest in the current model. Owing to the fact that cloud processes and surface albedo effect are intricately related at high latitudes, more research is needed to disentangle their roles and the uncertainties. Moreover, the PRP method, which was often used to quantify the strengths of different feedbacks (e.g., Colman et al. 1997), fails to separate the changes in cloud fields resulting from indirect effects (microphysically induced in nature) from the traditional dynamically induced cloud response. Thus, one cannot apply it without modification to study cloud feedback any more. On the other hand, the PRP-based strengths of the noncloud feedbacks (viz., albedo, lapse rate, and water vapor) in GAS are within 5% of those in AERO, indicating that they probably behave linearly irrespective of the signs, magnitudes, and geographical distributions of the perturbations. This leads us to believe that the cloud response is the most likely source of the nonlinearity in the present integrations.

The changes in precipitation pattern from a simultaneous increase in aerosols and gases are characteristic of drier conditions north of the equator and wetter conditions to the south, prompted by a southward shift of ITCZ as in AERO (Fig. 13). They are distinct from the response to radiatively active gases, which generally increase precipitation in the tropics, especially between the equator and 10°N. This is a clear indication of the role of aerosols in effectively altering the location of ITCZ resulting from the uneven distribution of the forcing between the hemispheres. The response to simultaneous increases in aerosols and radiatively active gases largely resembles that solely from aerosols in terms of pattern, except for slight northward shifts. Moreover, the presence of radiatively active gases tends to strengthen the shift of ITCZ in terms of the magnitude south of 10°N. This is contrary to a slight damping suggested by the arithmetic sum of AERO and GAS. This may suggest that aerosols have a stronger impact on precipitation than gases as a result of the former's roles in altering surface SW fluxes.

4. Discussion

The results here can be compared to those of Feichter et al. (2004). Their model implemented a prognostic scheme of cloud droplet number concentration (Lohmann et al. 1999, 2000) and online aerosol chemistry, and was coupled to a mixed layer ocean model to simulate climate response to aerosols and WMGG. Although that study's results are similar to the present work in suggesting that the increase in global annual mean surface temperature from WMGG and aerosols is significantly smaller than that obtained by adding up the individual responses, the spatial patterns of the responses differ. The nonlinearity is found at all latitudes in Feichter et al. (2004), but is concentrated mainly in NH in this study. The latter finding seems consistent with the NH–SH distribution of aerosol forcing. Because aerosols have a much weaker effect than radiatively active gases in SH, the resulting nonlinearity, if any, should presumably be smaller there than in NH. Note that the simulated cooling caused by aerosols is confined largely to the NH (e.g., Fig. 3 in Feichter et al. 2004; Fig. 1 in this work). Although Feichter et al. (2004) showed that the nonlinear cloud response is the main explanation in a global mean sense, it is unclear whether this would be true for all the latitudes and what roles surface albedo feedback may play. Thus, we make no attempt to further compare these two studies on the regional scale other than noting that the nonlinearity is associated with cloud feedback in our study. Also, this could be indicative of the results depending on parameterizations in the different models.

Feichter et al. (2004) reported a global mean hydrological sensitivity (percentage change in precipitation per 1-K change in surface temperature) of 3.9% K^{-1} for aerosols and 1.5% K^{-1} for WMGG. The reason why precipitation is substantially more susceptible to aerosols than to WMGG is that the former is more effective in altering surface radiation energy available for water evaporation than the latter (Feichter et al. 2004; Lohmann and Feichter 2005). This also explains the negative hydrological sensitivity (-1.9% K^{-1}) when both are combined. This study confirms these findings, with the hydrological sensitivity calculated at 3.0% K^{-1} for aerosols, 1.7% K^{-1} for radiatively active gases, and -2.4% K^{-1} for both. However, it does not support the argument in Feichter et al. (2004) that the nonlinearity in hydrological response is the consequence of feedback of meteorology on aerosol burden. Note that prescribed aerosols are used in this work.

Krisjánsson et al. (2005) discussed in detail the response of cloud fields to aerosol effects in Community Climate Model (CCM)-Oslo, and suggested that reduced

moisture in a colder climate gives rise to the lowering of LWP and cloud amount at high latitudes, in addition to reducing the increase in LWP caused by the second indirect effect at the NH midlatitudes. The global mean effect is a net decrease in LWP. This is opposite to the present result, showing an overall increase in LWP. Although this study agrees with Krisjánsson et al. (2005) in finding decreased specific humidity in response to aerosols, the relative humidity generally increases at the model layers below around 400 mbar outside the tropics because of the tropospheric cooling, while decreasing above partly results from stratospheric warming. This alone would tend to increase slightly the cloud condensate and amount in the troposphere. On the contrary, LWP also decreases at high latitudes despite the second indirect effect in this study (Fig. 6). Jones et al. (2007) attributed the same phenomenon (see their Fig. 9a) to more liquid freezing in mixed-phase clouds at lower temperature (the freezing effect). If this is the main process involved without considering possible changes in total condensate, IWP would increase. However, both Krisjánsson et al. (2005) and this study show simultaneous reduction in LWP and IWP at high latitudes, which Krisjánsson et al. (2005) argued indicates that less moisture suppresses liquid and ice clouds (thus total condensate) alike. Thus, the explanation given in Jones et al. (2007) does not hold for this study. As discussed in section 3a, the dq_s/dT effect, and to a lesser extent the freezing effect, is responsible for high-latitude cloud response in this study. Because total condensate at high latitudes increases in Jones et al. (2007, see their Fig. 11a), IWP must increase in light of the decrease in LWP. The reason why their study differs from that of Krisjánsson et al. (2005) and this work in this aspect is unclear.

5. Conclusions

A modified version of the GFDL AM2.1 with a prognostic treatment of aerosol indirect effects is coupled to a mixed layer ocean model to study the climate response to anthropogenic aerosols. The surface temperature reduces by 1.9 K in response to anthropogenic aerosols. The troposphere cools as well, while the stratosphere warms. Interhemispheric asymmetry in the model's thermal response (i.e., the Northern Hemisphere cools more than the Southern Hemisphere) yields a southward shift of ITCZ, thus substantially reducing precipitation north of the equator while increasing it to the south. The significant reduction in SW surface radiation gives rise to a net decrease in evaporation (as well as precipitation). When being subject to anthropogenic aerosols and radiatively active gases simultaneously, the model response shows some degree of nonlinearity. The increase in surface temperature (0.55 K) is significantly less than the sum of the individual responses to aerosol and gas effects (0.86 K). NH undergoes a nearly complete offset between aerosol and gas effects, while SH is dominated by gas effect. The model's response is also characteristic of the nonlinear changes in cloud fields that are amplified through surface albedo feedback at high latitudes. Both factors play important roles in affecting regional responses. The change in precipitation pattern arising from the simultaneous increases in aerosols and gases largely resembles that in response to aerosols only, while the magnitude of the shift of ITCZ is further strengthened relative to that case south of 10°N. Note that the equilibrium response discussed in this paper could differ from the transient response in many aspects, and thus cannot be applied directly to interpret the observed temperature trend. The latter can be reliably assessed only by running a fully coupled AOGCM driven by historical forcings.

Acknowledgments. We thank Ronald Stouffer, Michael Winton, and two anonymous reviewers for helpful comments.

REFERENCES

Albrecht, B., 1989: Aerosols, cloud microphysics, and fractional cloudiness. *Science,* **245,** 1227–1230.

Alexeev, V. A., P. L. Langen, and J. R. Bates, 2005: Polar amplification of surface warming on an aquaplanet in ''ghost forcing'' experiments without sea ice feedbacks. *Climate Dyn.,* **24,** 655–666.

Andreae, M. O., C. D. Jones, and P. M. Cox, 2005: Strong present-day aerosol cooling implies a hot future. *Nature,* **435,** 1187–1190.

Boucher, O., and U. Lohmann, 1995: The sulphate-CCN-cloud albedo effect—A sensitivity study with two general circulation models. *Tellus,* **47B,** 281–300.

Broccoli, A. J., K. A. Dahl, and R. J. Stouffer, 2006: Response of the ITCZ to Northern Hemisphere cooling. *Geophys. Res. Lett.,* **33,** L01702, doi:10.1029/2005GL024546.

Cai, W., T. Cowan, M. Dix, L. Rotstayn, J. Ribbe, G. Shi, and S. Wijffels, 2007: Anthropogenic aerosol forcing and the structure of temperature trends in the southern Indian Ocean. *Geophys. Res. Lett.,* **34,** L14611, doi:10.1029/2007GL030380.

Chen, C.-T., and V. Ramaswamy, 1996: Sensitivity of simulated global climate to perturbations in low cloud microphysical properties. Part II: Spatially localized perturbations. *J. Climate,* **9,** 2788–2801.

Colman, R. A., S. B. Power, and B. J. McAvaney, 1997: Non-linear climate feedback analysis in an atmospheric general circulation model. *Climate Dyn.,* **13,** 717–731.

Delworth, T. L., and K. W. Dixon, 2006: Have anthropogenic aerosols delayed a greenhouse gas-induced weakening of the North Atlantic thermohaline circulation? *Geophys. Res. Lett.,* **33,** L02606, doi:10.1029/2005GL024980.

——, and Coauthors, 2006: GFDL's CM2 global coupled climate models. Part I: Formulation and simulation characteristics. *J. Climate,* **19,** 643–674.

Feichter, J., E. Roeckner, U. Lohmann, and B. Liepert, 2004: Nonlinear aspects of the climate response to greenhouse gas and aerosol forcing. *J. Climate,* **17,** 2384–2398.

GFDL Global Atmospheric Model Development Team, 2004: The new GFDL global atmosphere and land model AM2–LM2: Evaluation with prescribed SST simulations. *J. Climate,* **17,** 4641–4673.

Hansen, J., A. Lacis, D. Rind, G. Russell, P. Stone, I. Fung, R. Ruedy, and J. Lerner, 1984: Climate sensitivity: Analysis of feedback mechanisms. *Climate Processes and Climate Sensitivity,* J. E. Hansen and T. Takahashi, Eds., Amer. Geophys. Union, 130–163.

——, M. Sato, and R. Ruedy, 1997: Radiative forcing and climate response. *J. Geophys. Res.,* **102,** 6831–6864.

——, and Coauthors, 2005: Efficacy of climate forcings. *J. Geophys. Res.,* **110,** D18104, doi:10.1029/2005JD005776.

Haywood, J. M., and V. Ramaswamy, 1998: Global sensitivity studies of the direct radiative forcing due to anthropogenic sulfate and black carbon aerosols. *J. Geophys. Res.,* **103,** 6043–6058.

Horowitz, L. W., 2006: Past, present, and future concentrations of tropospheric ozone and aerosols: Methodology, ozone evaluation, and sensitivity to aerosol wet removal. *J. Geophys. Res.,* **111,** D22211, doi:10.1029/2005JD006937.

Jones, A., J. M. Haywood, and O. Boucher, 2007: Aerosol forcing, climate response and climate sensitivity in the Hadley Centre climate model. *J. Geophys. Res.,* **112,** D20211, doi:10.1029/2007JD008688.

Krisjánsson, J. E., T. Iversen, A. Kirkevåg, Ø. Seland, and J. Debernard, 2005: Response of the climate system to aerosol direct and indirect forcing: Role of cloud feedbacks. *J. Geophys. Res.,* **110,** D24206, doi:10.1029/2005JD006299.

Lin, S.-J., 2004: A ''vertically Lagrangian'' finite-volume dynamical core for global models. *Mon. Wea. Rev.,* **132,** 2293–2307.

Lohmann, U., and J. Feichter, 2005: Global indirect aerosol effects: A review. *Atmos. Chem. Phys.,* **5,** 715–737.

——, ——, C. C. Chuang, and J. E. Penner, 1999: Predicting the number of cloud droplets in the ECHAM GCM. *J. Geophys. Res.,* **104,** 9169–9198.

——, ——, J. E. Penner, and R. Leaitch, 2000: Indirect effect of sulfate and carbonaceous aerosols: A mechanistic treatment. *J. Geophys. Res.,* **105,** 12 193–12 206.

Manabe, S., and R. J. Stouffer, 1980: Sensitivity of a global climate model to an increase of CO_2 concentration in the atmosphere. *J. Geophys. Res.,* **85,** 5529–5554.

Milly, P. C. D., and A. B. Shmakin, 2002: Global modeling of land water and energy balances. Part I: The land dynamics (LaD) model. *J. Hydrometeor.,* **3,** 283–299.

Ming, Y., V. Ramaswamy, L. J. Donner, and V. T. J. Phillips, 2006: A new parameterization of cloud droplet activation applicable to general circulation models. *J. Atmos. Sci.,* **63,** 1348–1356.

——, ——, ——, ——, S. A. Klein, P. A. Ginoux, and L. W. Horowitz, 2007: Modeling the interactions between aerosols and liquid water clouds with a self-consistent cloud scheme in a general circulation model. *J. Atmos. Sci.,* **64,** 1189–1209.

Mitchell, J. F. B., and T. C. Johns, 1997: On modification of global warming by sulfate aerosols. *J. Climate,* **10,** 245–267.

Raisanen, J., 1998: CO_2- and aerosol-induced changes in vertically integrated zonal momentum budget in a GCM experiment. *J. Climate,* **11,** 625–639.

Ramanathan, V., P. J. Crutzen, J. T. Kiehl, and D. Rosenfeld, 2001: Aerosols, climate and the hydrological cycle. *Science,* **294,** 2119–2124.

Ramaswamy, V., and C.-T. Chen, 1997: Linear additivity of climate response for combined albedo and greenhouse perturbations. *Geophys. Res. Lett.,* **24,** 567–570.

——, and Coauthors, 2001: Radiative forcing of climate change. *Climate Change 2001: The Scientific Basis,* J. T. Houghton et al., Eds., Cambridge University Press, 349–416.

Randel, W. J., and F. Wu, 1999: A stratospheric ozone trends data set for global modeling studies. *Geophys. Res. Lett.,* **26,** 3089–3092.

Rotstayn, L. D., and J. E. Penner, 2001: Indirect aerosol forcing, quasi forcing, and climate response. *J. Climate,* **14,** 2960–2975.

——, and U. Lohmann, 2002: Tropical rainfall trends and the indirect aerosol effect. *J. Climate,* **15,** 2103–2116.

——, and Coauthors, 2007: Have Australian rainfall and cloudiness increased due to the remote effects of Asian anthropogenic aerosols? *J. Geophys. Res.,* **112,** D09202, doi:10.1029/2006JD007712.

Soden, B. J., and I. M. Held, 2006: An assessment of climate feedbacks in coupled ocean–atmosphere models. *J. Climate,* **19,** 3354–3360.

Stouffer, R. J., and Coauthors, 2006: GFDL's CM2 global coupled climate models. Part IV: Idealized climate response. *J. Climate,* **19,** 723–740.

Takemura, T., Y. Tsushima, T. Yokohata, T. Nozawa, T. Nagashima, and T. Nakajima, 2006: Time evolutions of various radiative forcings for the past 150 years estimated by a general circulation model. *Geophys. Res. Lett.,* **33,** L19705, doi:10.1029/2006GL026666.

Tiedtke, M., 1993: Representation of clouds in large-scale models. *Mon. Wea. Rev.,* **121,** 3040–3061.

Twomey, S., 1977: Influence of pollution on the short-wave albedo of clouds. *J. Atmos. Sci.,* **34,** 1149–1152.

Wetherald, R. T., and S. Manabe, 1988: Cloud feedback processes in a general circulation model. *J. Atmos. Sci.,* **45,** 1397–1415.

Williams, K. D., A. Jones, D. L. Roberts, C. A. Senior, and M. J. Woodage, 2001: The response of the climate system to the indirect effects of anthropogenic sulfate aerosol. *Climate Dyn.,* **17,** 845–856.

Winton, M., 2000: A reformulated three-layer sea ice model. *J. Atmos. Oceanic Technol.,* **17,** 525–531.

——, 2006: Amplified Arctic climate change: What does surface albedo feedback have to do with it? *Geophys. Res. Lett.,* **33,** L03701, doi:10.1029/2005GL025244.

Wyant, M. C., C. S. Bretherton, J. T. Backmeister, J. T. Kiehl, I. M. Held, M. Zhao, S. A. Klein, and B. J. Soden, 2006: A comparison of low-latitude cloud properties and their response to climate change in three AGCMs sorted into regimes using mid-tropospheric vertical velocity. *Climate Dyn.,* **27,** 261–279.